Machine Tool Genome Project: Tool point dynamics prediction for improved milling productivity

Tony L. Schmitz
University of North Carolina at Charlotte
Charlotte, NC, USA

Abstract
The Machine Tool Genome Project is described in this paper. In this project, Receptance Coupling Substructure Analysis (RCSA) is applied to predict the tool point dynamics for arbitrary tool-holder-spindle-machine combinations. This reduces the measurement time required using traditional modal testing techniques. In the RCSA approach, the tool-holder-spindle-machine assembly is considered as three separate components: the tool, holder, and spindle-machine and the individual frequency response functions (FRFs) for these components are coupled analytically. The archived measurement of the spindle-machine FRF (or receptance) is coupled to the free-free boundary condition receptances of the tool and the holder derived from Timoshenko beam models. An overview of the RCSA technique is presented and experimental results are presented.

Keywords
Milling, dynamics, receptance coupling, chatter

Introduction
Time and frequency domain milling process models may be implemented to enable pre-process parameter selection for optimized performance. To enable accurate process performance prediction using these models, the tool-holder-spindle-machine structural dynamics must be known [1-3]. The required tool point frequency response function (FRF) can be obtained by modal testing. However, for the large number of tool-holder combinations in typical production facilities, the measurements can be prohibitively time-consuming and costly.

In the Machine Tool Genome Project (MTGP), Receptance Coupling Substructure Analysis (RCSA) is applied as an alternative to modal testing [4-8]. In the RCSA approach, the tool-holder-spindle-machine assembly is considered as three separate components: the tool, holder, and spindle-machine and the individual FRFs of these components are coupled analytically. The archived measurement of the spindle-machine FRF (or receptance) is coupled to the free-free boundary condition receptances of the tool and the holder derived from Timoshenko beam models. In the MTGP paradigm, the tool, holder, and spindle-machine are considered as "genes". RCSA provides the "mapping" step to predict the "body characteristic" (assembly FRF). This paper presents a description of the MTGP and the RCSA mapping tool. Additionally, experimental results that demonstrate the utility of the MTGP to pre-process milling parameter selection are provided.

RCSA background
In the three-component RCSA model applied here [7], the tool and holder receptances are determined from beam models and the spindle-machine receptances are measured by impact testing. These substructure receptances are then joined analytically to obtain the assembly receptance as reflected at the tool point.

Figure 1 depicts the three individual components of the tool-holder-spindle-machine assembly: the tool (I), the holder (II), and the spindle-machine (III). Both the tool and holder are described using Timoshenko beam models (based on the geometry and material properties) with free-free boundary conditions [9]. The free-free tool and holder models are then coupled to form the subassembly I-II identified in Fig. 2, where $u_i = \{x_i \quad \theta_i\}^T$ are the component generalized coordinates composed of both a displacement, x_i, and a rotation, θ_i, and $U_i = \{X_i \quad \Theta_i\}^T$ are the assembly generalized coordinates. To couple components I and II, the coordinate definitions provided in Fig. 1 are applied, where $q_i = \{f_i \quad m_i\}^T$ are the component generalized forces composed of both a force, f_i, and a moment (or couple), m_i, and $Q_1 = \{F_1 \quad M_1\}^T$ is the assembly generalized force applied at assembly coordinate 1. The component I receptances include: 1) the direct receptances at the free end $h_{11} = \frac{x_1}{f_1}$, $l_{11} = \frac{x_1}{m_1}$, $n_{11} = \frac{\theta_1}{f_1}$, and $p_{11} = \frac{\theta_1}{m_1}$; 2) the cross receptances from the free end to the fixed end

(connected to the holder) $h_{12a} = \frac{x_1}{f_{2a}}$, $l_{12a} = \frac{x_1}{m_{2a}}$, $n_{12a} = \frac{\theta_1}{f_{2a}}$, and $p_{12a} = \frac{\theta_1}{m_{2a}}$; 3) the direct receptances at the fixed end $h_{2a2a} = \frac{x_{2a}}{f_{2a}}$, $l_{2a2a} = \frac{x_{2a}}{m_{2a}}$, $n_{2a2a} = \frac{\theta_{2a}}{f_{2a}}$, and $p_{2a2a} = \frac{\theta_{2a}}{m_{2a}}$; and 4) the cross receptances from the fixed end to the free end $h_{2a1} = \frac{x_{2a}}{f_1}$, $l_{2a1} = \frac{x_{2a}}{m_1}$, $n_{2a1} = \frac{\theta_{2a}}{f_1}$, and $p_{2a1} = \frac{\theta_{2a}}{m_1}$. These are organized into the generalized component receptance matrices, $R_{ij} = \begin{bmatrix} h_{ij} & l_{ij} \\ n_{ij} & p_{ij} \end{bmatrix}$, where $\{u_i\} = [R_{ij}]\{q_j\}$. For component II, the same receptances must be calculated using the Timoshenko beam model, but coordinate 1 is replaced with 2*b* and coordinate 2*a* is replaced with 3*a*. By assuming a rigid coupling between these two components, the I-II subassembly tip receptances: (direct) G_{11} and G_{3a3a}; and (cross) G_{13a} and G_{3a1} can be determined, where $G_{ij} = \begin{bmatrix} H_{ij} & L_{ij} \\ N_{ij} & P_{ij} \end{bmatrix}$ are the generalized assembly receptance matrices and $\{U_i\} = [G_{ij}]\{Q_j\}$.

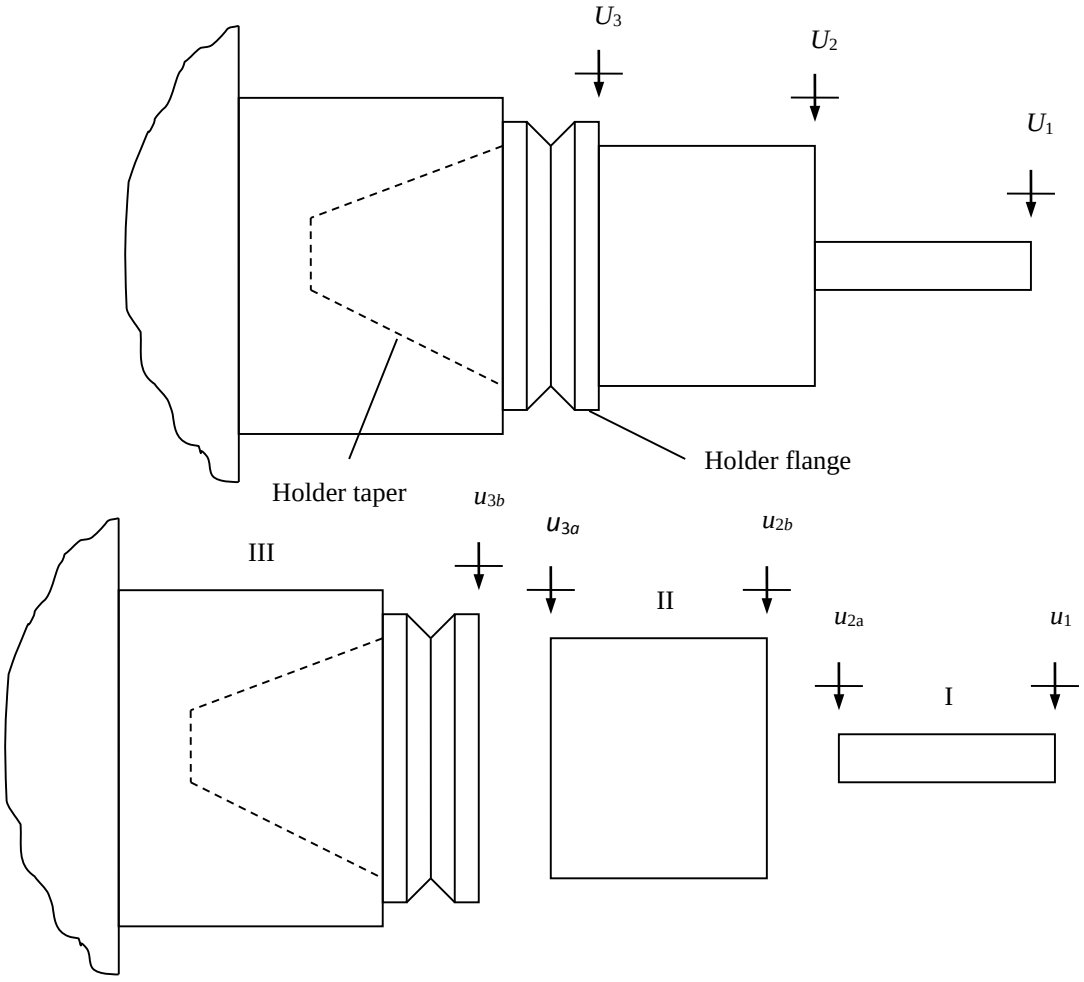

Figure 1: Three-component receptance coupling model of tool (I), holder (II), and spindle-machine (III).

To determine the direct and cross receptances at the right end of the subassembly, G_{11} and G_{3a1}, Q_1 is applied to coordinate U_1 as shown in Fig. 3. The components' displacements/rotations are: $u_1 = R_{11}q_1 + R_{12a}q_{2a}$, $u_{2a} = R_{2a1}q_1 + R_{2a2a}q_{2a}$, $u_{2b} = R_{2b2b}q_{2b}$, and $u_{3a} = R_{3a2b}q_{2b}$. The equilibrium conditions are: $q_{2a} + q_{2b} = 0$ and $q_1 = Q_1$. The component displacements/rotations and equilibrium conditions are substituted into the compatibility

condition for the rigid connection, $u_{2b} - u_{2a} = 0$, to obtain the expression for q_{2b} shown in Eq. 1. The component force q_{2a} is then determined from the equilibrium condition $q_{2a} = -q_{2b}$. The expression for G_{11} is provided in Eq. 2. The cross receptance matrix G_{3a1} is shown in Eq. 3.

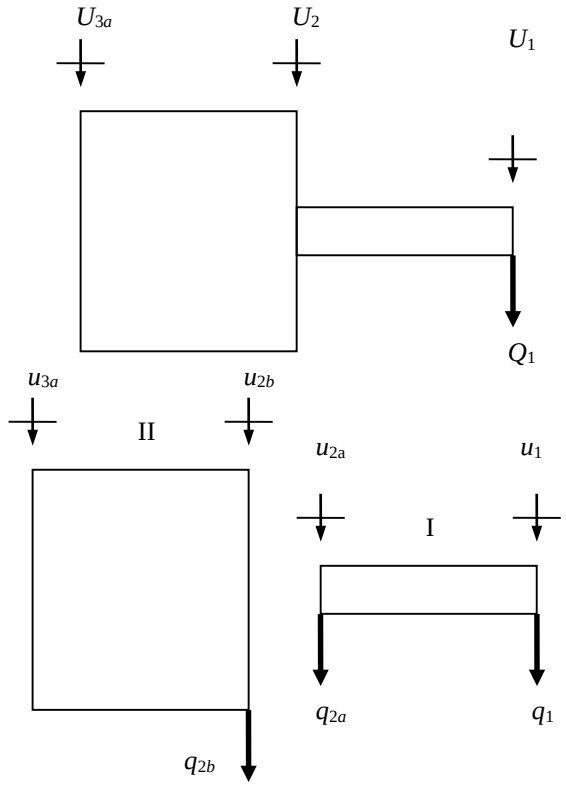

Figure 2: Subassembly I-II composed of tool (I) and holder (II). The generalized force Q_1 is applied to U_1 to determine G_{11} and G_{3a1}.

$$\begin{aligned} & u_{2b} - u_{2a} = 0 \\ & R_{2b2b} q_{2b} - R_{2a1} q_1 - R_{2a2a} q_{2a} = 0 \\ & \left(R_{2a2a} + R_{2b2b}\right) q_{2b} - R_{2a1} Q_1 = 0 \\ & q_{2b} = \left(R_{2a2a} + R_{2b2b}\right)^{-1} R_{2a1} Q_1 \end{aligned} \tag{1}$$

$$\begin{aligned} & G_{11} = \frac{U_1}{Q_1} = \frac{u_1}{Q_1} = \frac{R_{11} q_1 + R_{12a} q_{2a}}{Q_1} = \frac{R_{11} Q_1 - R_{12a}\left(R_{2a2a} + R_{2b2b}\right)^{-1} R_{2a1} Q_1}{Q_1} \\ & G_{11} = R_{11} - R_{12a}\left(R_{2a2a} + R_{2b2b}\right)^{-1} R_{2a1} = \begin{bmatrix} H_{11} & L_{11} \\ N_{11} & P_{11} \end{bmatrix} \end{aligned} \tag{2}$$

$$\begin{aligned} & G_{3a1} = \frac{U_{3a}}{Q_1} = \frac{u_{3a}}{Q_1} = \frac{R_{3a2b} q_{2b}}{Q_1} = \frac{R_{3a2b}\left(R_{2a2a} + R_{2b2b}\right)^{-1} R_{2a1} Q_1}{Q_1} \\ & G_{3a1} = R_{3a2b}\left(R_{2a2a} + R_{2b2b}\right)^{-1} R_{2a1} = \begin{bmatrix} H_{3a1} & L_{3a1} \\ N_{3a1} & P_{3a1} \end{bmatrix} \end{aligned} \tag{3}$$

To find the remaining tip receptances, G_{3a3a} and G_{13a}, Q_{3a} is applied to assembly coordinate U_{3a}. Following the same approach, the equations for the direct receptance G_{3a3a} (Eq. 4) and the cross receptance G_{13a} (Eq. 5) are determined.

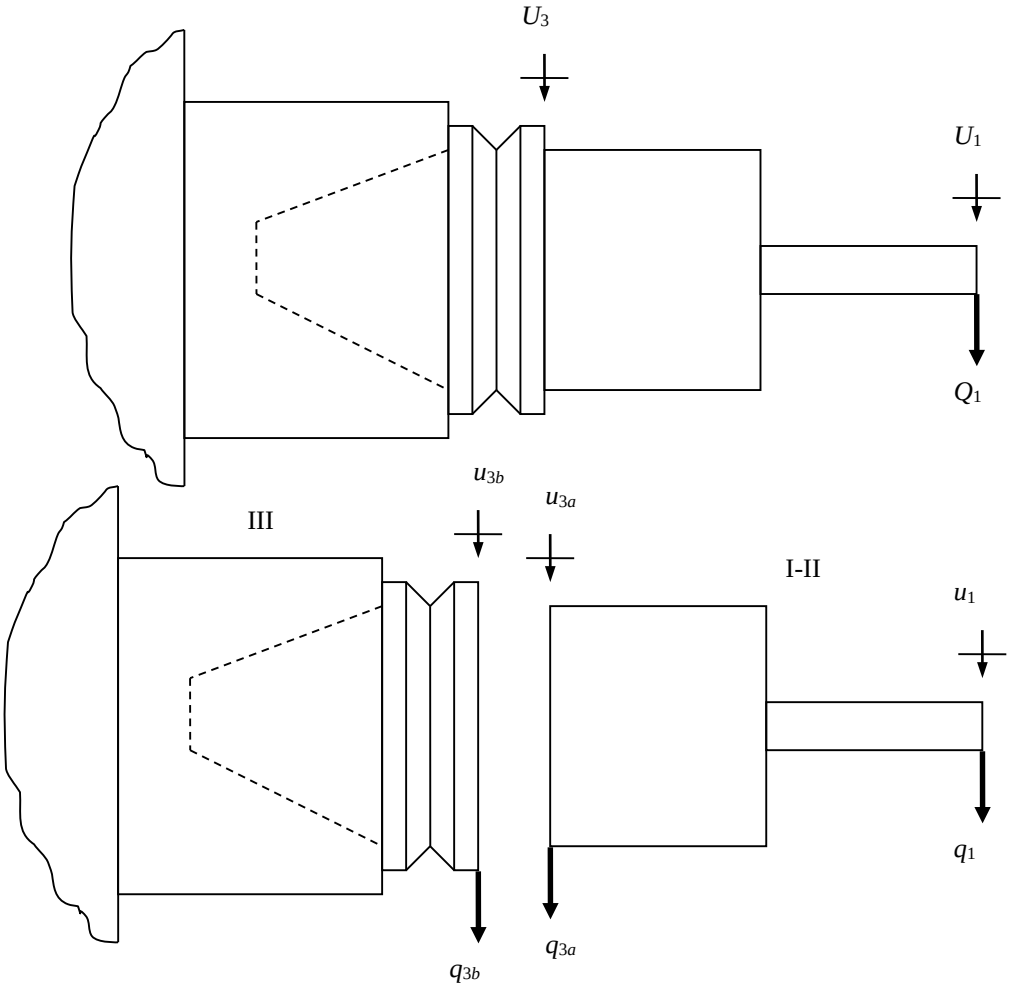

Figure 3: The I-II subassembly is rigidly coupled to the spindle-machine (III) to determine the tool point receptance matrix, G_{11}.

$$
\begin{aligned}
G_{3a3a} &= \frac{U_{3a}}{Q_{3a}} = \frac{u_{3a}}{Q_{3a}} = \frac{R_{3a3a}q_{3a} + R_{3a2b}q_{2b}}{Q_{3a}} \\
G_{3a3a} &= \frac{R_{3a3a}Q_{3a} - R_{3a2b}\left(R_{2a2a} + R_{2b2b}\right)^{-1}R_{2b3a}Q_{3a}}{Q_{3a}} \\
G_{3a3a} &= R_{3a3a} - R_{3a2b}\left(R_{2a2a} + R_{2b2b}\right)^{-1}R_{2b3a} = \begin{bmatrix} H_{3a3a} & L_{3a3a} \\ N_{3a3a} & P_{3a3a} \end{bmatrix}
\end{aligned}
\tag{4}
$$

$$
\begin{aligned}
G_{13a} &= \frac{U_1}{Q_{3a}} = \frac{u_1}{Q_{3a}} = \frac{R_{12a}q_{2a}}{Q_{3a}} = \frac{R_{12a}\left(R_{2a2a} + R_{2b2b}\right)^{-1}R_{2b3a}Q_{3a}}{Q_{3a}} \\
G_{13a} &= R_{12a}\left(R_{2a2a} + R_{2b2b}\right)^{-1}R_{2b3a} = \begin{bmatrix} H_{13a} & L_{13a} \\ N_{13a} & P_{13a} \end{bmatrix}
\end{aligned}
\tag{5}
$$

Once the free-free components I and II are coupled to form the subassembly I-II, this subassembly is then rigidly coupled to the spindle-machine to give the assembly tool point receptances, G_{11}; see Fig. 3. This coupling is carried out using Eq. 6:

$$G_{11} = R_{11} - R_{13a}\left(R_{3a3a} + R_{3b3b}\right)^{-1} R_{3a1}, \tag{6}$$

where the R_{ij} matrices are the subassembly matrices from the I-II coupling result. Therefore, $R_{11} = G_{11}$ from Eq. 2, $R_{3a1} = G_{3a1}$ from Eq. 3, $R_{3a3a} = G_{3a3a}$ from Eq. 4, and $R_{13a} = G_{13a}$ from Eq. 5. The remaining unknown in Eq. 6 is the spindle-machine receptance matrix, R_{3b3b}.

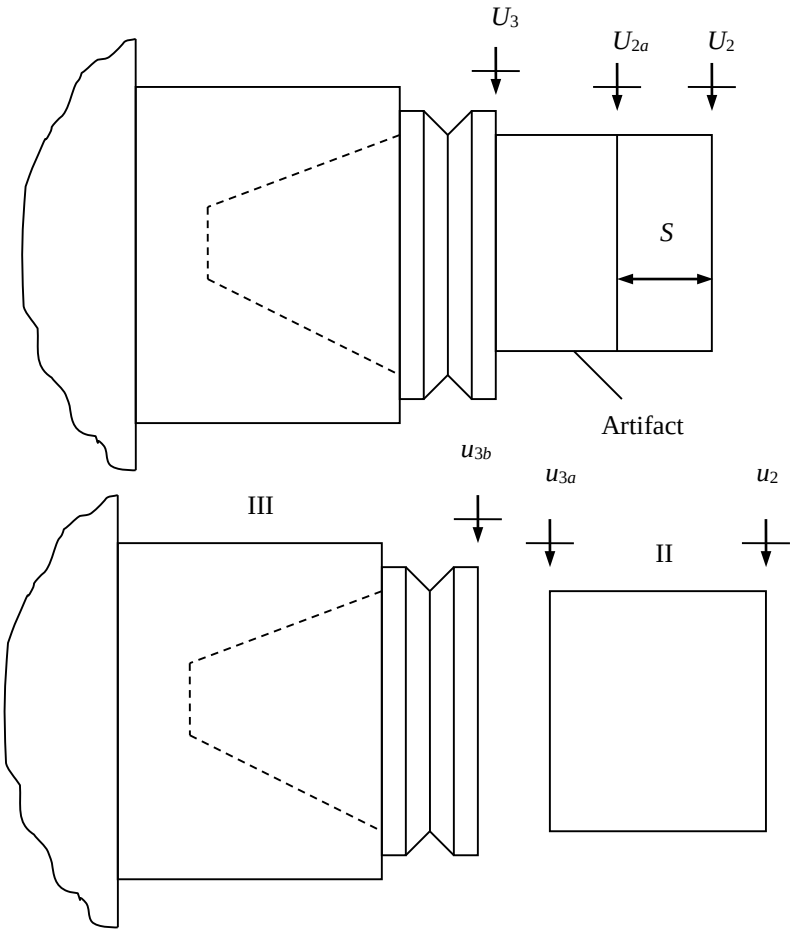

Figure 4: Artifact model for determining R_{3b3b} by inverse RCSA.

Inverse RCSA

In order to identify R_{3b3b} for Eq. 6 experimentally, a measurement artifact that includes not only the flange and taper, but also incorporates some length beyond the flange is inserted into the spindle; see Fig. 4. The assembly matrix $G_{22} = \begin{bmatrix} H_{22} & L_{22} \\ N_{22} & P_{22} \end{bmatrix}$ is determined experimentally and then the portion of the artifact beyond the flange is removed in simulation to isolate R_{3b3b}. The free end response for the artifact-spindle-machine assembly is described by Eq. 7, where the R_{22}, R_{23a}, R_{3a3a}, and R_{3a2} matrices are populated using a beam model of the portion of the artifact beyond the flange. Equation 7 is rearranged in Eq. 8 to isolate R_{3b3b}. This step of decomposing the measured assembly receptances, G_{22}, into the modeled substructure receptances, R_{3a2}, R_{22}, R_{23a} , and R_{3a3a}, and spindle-machine receptances, R_{3b3b}, is referred to as “inverse RCSA”.

$$G_{22} = R_{22} - R_{23a}\left(R_{3a3a} + R_{3b3b}\right)^{-1} R_{3a2} \tag{7}$$

$$
\begin{aligned}
G_{22} - R_{22} &= -R_{23a}\left(R_{3a3a} + R_{3b3b}\right)^{-1} R_{3a2} \\
R_{23a}{}^{-1}\left(R_{22} - G_{22}\right)R_{3a2}{}^{-1} &= \left(R_{3a3a} + R_{3b3b}\right)^{-1} \\
R_{3a2}\left(R_{22} - G_{22}\right)^{-1} R_{23a} &= R_{3a3a} + R_{3b3b} \\
R_{3b3b} &= R_{3a2}\left(R_{22} - G_{22}\right)^{-1} R_{23a} - R_{3a3a}
\end{aligned}
\tag{8}
$$

The experimental identification of the four receptances that make up the G_{22} matrix is described in [8]. In short, the H_{22} receptance is measured and then each mode in the measurement bandwidth is fit using a fixed-free, cylindrical Euler-Bernoulli beam model; see Eq. 9, where $\lambda^4 = \omega^2 \frac{\rho A}{EI\left(1+i\eta\right)}$, $A = \frac{\pi d^2}{4}$, $I = \frac{\pi d^4}{64}$, ω is frequency (rad/s), ρ is the density, E is the elastic modulus, η is the solid damping factor (unitless), d is the beam diameter, and L is the beam length. Given the length, diameter, and solid damping factor for each mode, the remaining receptances are described using Eqs. 10-11.

$$
H_{22} = \frac{\sin\left(\lambda L\right)\cosh\left(\lambda L\right) - \cos\left(\lambda L\right)\sinh\left(\lambda L\right)}{\lambda^3 EI\left(1+i\eta\right)\left(\cos\left(\lambda L\right)\cosh\left(\lambda L\right) - 1\right)} \tag{9}
$$

$$
L_{22} = N_{22} = \frac{-\sin\left(\lambda L\right)\sinh\left(\lambda L\right)}{\lambda^2 EI\left(1+i\eta\right)\left(\cos\left(\lambda L\right)\cosh\left(\lambda L\right) - 1\right)} \tag{10}
$$

$$
P_{22} = \frac{\cos\left(\lambda L\right)\sinh\left(\lambda L\right) + \sin\left(\lambda L\right)\cosh\left(\lambda L\right)}{\lambda EI\left(1+i\eta\right)\left(\cos\left(\lambda L\right)\cosh\left(\lambda L\right) - 1\right)} \tag{11}
$$

Tool point receptance prediction

In this study, the spindle-machine receptances for a Mikron UPC-600 Vario CNC milling machine spindle (HSK-63A interface) were identified using the Euler-Bernoulli approach. These receptances were then coupled to models of two tool-holder combinations to predict the tool point receptances.

A three flute, 25.4 mm diameter carbide endmill was clamped in a (thermal) shrink fit tool holder. After inserting this subassembly in the Mikron UCP-600 Vario spindle, the tool point receptance, H_{11}, was measured by impact testing and compared to predictions. The dimensions for the Timoshenko beam tool-holder model are provided in Fig. 5 for an overhang length of 86.9 mm. The fluted portion of the tool was modeled using an equivalent diameter, where this diameter was obtained by weighing the carbide tool, assuming a density (15000 kg/m^3), and calculating the solid section equivalent flute diameter based on the cylindrical dimensions and the tool and flute lengths. The elastic modulus for the Timoshenko beam model was 550 GPa and Poisson's ratio was 0.22. The prediction and measurement are presented in Fig. 6. The overhang length was then extended to 107 mm and the exercise was repeated. The results are shown in Fig. 7.

Conclusions

The Machine Tool Genome Project was described. In this project, Receptance Coupling Substructure Analysis (RCSA) is applied to predict the tool point dynamics for arbitrary tool-holder-spindle-machine combinations as an alternative to modal testing. In the RCSA approach, the tool-holder-spindle-machine assembly is considered as three separate components: the tool, holder, and spindle-machine and the individual FRFs of these components are coupled analytically. The archived measurement of the spindle-machine FRF (or receptance) is coupled to the free-free boundary condition receptances of the tool and the holder derived from beam models. A description of the RCSA technique was presented and experimental results were included to demonstrate the ability of the MTGP to provided pre-process milling parameter selection.

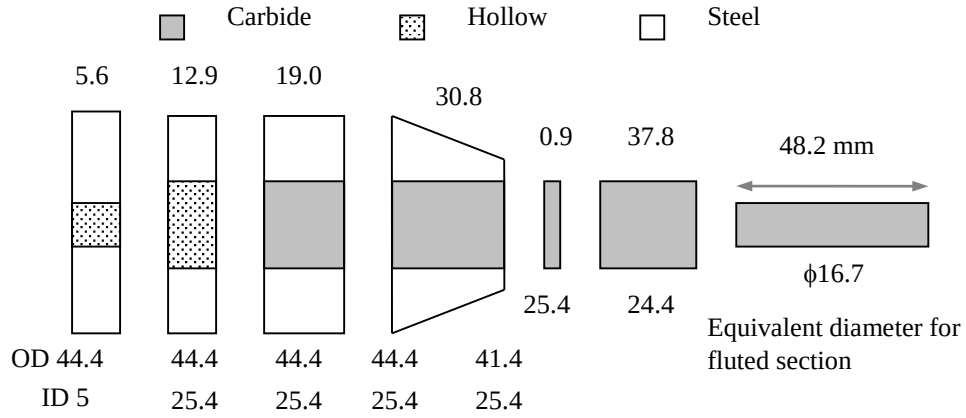

Figure 5: Beam model for 25.4 mm diameter, three flute endmill inserted in a tapered shrink fit holder (not to scale). The overhang length is 86.9 mm.

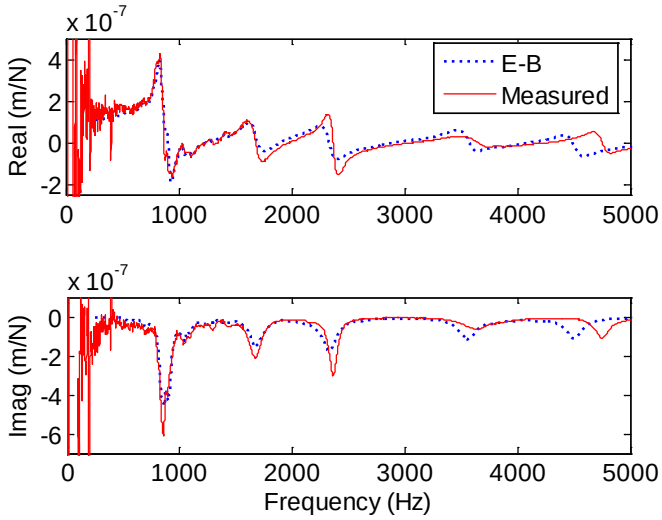

Figure 6: Comparison between H_{11} tool point measurement and Euler-Bernoulli (E-B) approach prediction for three flute, 25.4 mm diameter endmill with an overhang length of 86.9 mm.

Acknowledgements
The author gratefully acknowledges financial support from the National Science Foundation through grant numbers CMMI-0928393 and CMMI-0928211. The author also recognizes the contributions of D. Barton, BlueSwarf, T. Delio, Manufacturing Laboratories, Inc., G.S. Duncan, Valparaiso University, and U. Kumar, GE Global Research.

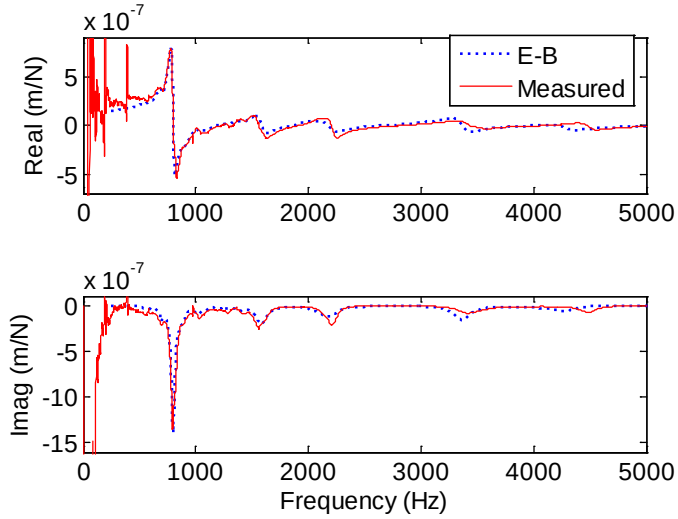

Figure 7: Comparison between H_{11} tool point measurement and E-B approach prediction for three flute, 25.4 mm diameter endmill with an overhang length of 107 mm.

References

1. Tlusty, J., 2000, Manufacturing Processes and Equipment, Prentice-Hall, Inc., Upper Saddle River, NJ.
2. Altintas, Y., 2000, Manufacturing Automation: Metal Cutting Mechanics, Machine Tool Vibrations, and CNC Design, Cambridge University Press, Cambridge, UK.
3. Schmitz, T. and Smith, K.S., 2009, Machining Dynamics: Frequency Response to Improved Productivity, Springer, New York, NY.
4. Schmitz, T. and Donaldson, R., 2000, Predicting High-Speed Machining Dynamics by Substructure Analysis, Annals of the CIRP, 49/1: 303-308.
5. Schmitz, T., Davies, M., Medicus, K., and Snyder, J., 2001, Improving High-Speed Machining Material Removal Rates by Rapid Dynamic Analysis, Annals of the CIRP, 50/1: 263-268.
6. Schmitz, T., Davies, M., and Kennedy, M., 2001, Tool Point Frequency Response Prediction for High-Speed Machining by RCSA, Journal of Manufacturing Science and Engineering, 123: 700-707.
7. Schmitz, T. and Duncan, G.S., 2005, Three-Component Receptance Coupling Substructure Analysis for Tool Point Dynamics Prediction, Journal of Manufacturing Science and Engineering, 127/4: 781-790.
8. Kumar, U. and Schmitz, T., 2012, Spindle Dynamics Identification for Receptance Coupling Substructure Analysis, Precision Engineering, 36/3: 435-443.
9. Weaver, Jr., W., Timoshenko, S., and Young, D., 1990, Vibration Problems in Engineering, 5th Edition, John Wiley and Sons, New York, NY.